*Desalination and Water Treatment*
www.deswater.com
doi: 10.1080/19443994.2014.942376

56 (2015) 327–337
October

Taylor & Francis
Taylor & Francis Group

# Performance of granular dead anaerobic sludge as permeable reactive barrier for containment of lead from contaminated groundwater

Abbas H. Sulaymon, Ayad A.H. Faisal, Ziad T. Abd Ali*

*Department of Environmental Engineering, College of Engineering, University of Baghdad, Baghdad, Iraq, Tel. +9647903971195; email: inas_abbas@yahoo.com (A.H. Sulaymon), Tel. +9647904208688; email: ayadabedalhamzafaisal@yahoo.com (A.A.H. Faisal), Tel. +9647903433954; email: z.teach2000@yahoo.com (Z.T. Abd Ali)*

Received 4 December 2013; Accepted 12 June 2014

ABSTRACT

This study investigates the performance of granular dead anaerobic sludge (GDAS) bio-sorbent as permeable reactive barrier (PRB) in removing lead from a contaminated shallow groundwater. Batch tests have been performed to characterize the equilibrium sorption properties of the GDAS and sandy soil in lead-containing aqueous solutions. A 1D advection–dispersion equation, solved by computer solutions Multiphysics 3.5a software which is based on finite element method, has been used to simulate the equilibrium transport of $Pb^{+2}$ ions within groundwater. This equation has taken into account the pollutant sorption onto the GDAS and sandy soil which is performed by Langmuir equation. Numerical results proved that the PRB plays a potential role in the restriction of the contaminant plume migration. These results also show that the thicker PRB is better than the thinner ones in lead treatment and the barrier starts to saturate with contaminant as a function of the travel time. A good agreement between the predicted and experimental results was recognized with root mean square error not exceeded the 0.0499.

*Keywords:* Granular dead anaerobic sludge; Lead; Permeable reactive barrier; Groundwater; Transport

## 1. Introduction

Contaminated groundwater is currently one of the major environmental problems facing the earth. There are many technologies to remediate contaminants in groundwater [1]. The most common technology used historically for remediation of groundwater has been ex situ pump-and-treat systems. These systems extract groundwater to the surface; treat it by different approaches such as: adsorption and either re-introduce the treated water to the subsurface or discharge it to a storm drain. This technique is difficult, costly and ineffective most of the time in removing enough contamination to restore the groundwater to drinking water standards in acceptable time frames [2–4]. Accordingly, permeable reactive barriers (PRBs) technology was alternative method used to remediate groundwater contaminated with different types of contaminants. It is found to be more cost effective than pump-and-treat. It has also been a demonstrated potential to diminish the spread of contaminants. The definition of PRBs according to the EPA as follows [5]:

*Corresponding author.

> an emplacement of reactive materials in the subsurface designed to intercept a contaminant plume, provide a flow path through the reactive media, and transform the contaminant(s) into environmentally acceptable forms to attain remediation concentration goals down gradient of the barrier

Considerable theoretical and experimental studies on PRBs using different types of reactive medium such as activated carbon, zeolite and zero-valent iron (ZVI) for treatment of heavy metals in groundwater have been achieved. For example, a set of batch and column tests were conducted to determine the design factors for clinoptilolite, one of the natural zeolites, PRBs against the contaminated groundwater by ammonium and heavy metals [6]. Effects of cold temperature on the ion-exchange equilibria of copper with clinoptilolite in natural and pretreated sodium forms were investigated [7]. Removal of heavy metal from contaminated groundwater is made possible on activated sludge by bio-sorption process which depended on the complex substance formed by the heavy metal and functional groups such as carboxyl, hydroxyl and phenolic of extracellular polymeric substance [8]. The potential application of activated carbon in permeable adsorbing barrier for the removal of cadmium was investigated. The adsorption isotherms of this material are experimentally determined and a theoretical model is proposed for the interpretation of experimental results [9]. The results of a column reactor test, aiming at evaluating the performance of a low-cost waste materials permeable barrier, for Cr(VI) removal from contaminated groundwater were presented. These materials were included green compost, produced as amendment for agricultural use, and siliceous gravel which tested as reactive medium in the experimental activity [10]. The potential use of the immobilized Mentha arvensis distillation waste biomass for removal and recovery of Cu(II) and Zn(II) from aqueous solution was evaluated [11]. A continuous column experiment was carried out under dynamic flow conditions in order to study the efficiency of low-cost PRBs to remove several inorganic contaminants from acidic solutions. A 50:50 w/w waste iron/sand mixture was used as candidate reactive media in order to activate precipitation and promote sorption and reduction–oxidation mechanisms [12]. The optimal weight ratio between iron and pumice in nickel removal from contaminated groundwater in order to balance the preservation of the hydraulic conductivity (favoured by increasing the pumice content of the mixture) and the removal efficiency (favoured by increasing ZVI content) was evaluated [13]. The performance of zeolite PRB in removing cadmium from a contaminated shallow aquifer was studied. Batch tests have been performed to characterize the equilibrium sorption properties of the zeolite in cadmium-containing aqueous solutions. A 1D numerical finite difference model was developed to describe pollutant transport within groundwater taking pollutant sorption on the PRB into account [14]. Many organic reactive materials such as agricultural products and by-products, sewage sludge and organic wastes [15–17] were used to study the metal removal from aqueous solutions under different conditions.

However, the regular biological activities of municipal wastewater treatment plants release large quantities of by-product biomass wastes, which represent both a solid waste and a pollutant. For example, this waste generated from Al-Rostomia'a third extension municipal treatment plant, Baghdad/Iraq was collected in 14 units of drying beds. The size of each unit was 350 m l × 25 m W ×1 m D. One can be expected the huge generated quantities of this material which be banished to the ecosystem. Thus, re-using of this waste as a reactive medium in PRBs is attractive in terms of sustainable development and reduced disposal costs.

Accordingly, the significance of the present study are: (1) investigating the potential application of granular dead anaerobic sludge (GDAS) bio-sorbent as an inexpensive material in PRBs for the removal of lead ($Pb^{2+}$) from the contaminated groundwater; (2) finding the predominant *functional* groups are responsible of $Pb^{2+}$ removal in the GDAS bio-sorbent depended on the Fourier transform infrared spectroscopy (FTIR) analysis; and (3) characterizing the 1D equilibrium transport of $Pb^{2+}$ theoretically, using computer solutions (COMSOL) Multiphysics 3.5a (2008) software, and experimentally *through simulated subsurface aquifer and GDAS barrier under saturated condition*.

## 2. Experimental work

### 2.1. Materials

The GDAS was dried at 25°C temperature for 5 d and then sieved into (1/0.6) mm diameter mesh. This portion was washed five times in distilled water and dried at 70°C for 6 h prior to usage [18]. Table 1 shows the physical and chemical characteristics of GDAS used in the present study.

The sandy soil, with composition and properties shown in Table 2, was used as aquifer in the conducted experiments. This soil had a particle size distribution ranged from 63 μm to 0.71 mm with an effective grain size, $d_{10}$, of 110 μm, a median grain

Table 1
Physical and chemical characteristics of GDAS

| | Value |
|---|---|
| Physical properties | |
| Actual density, (kg/m$^3$) | 1,742 |
| Apparent density, (kg/m$^3$) | 610 |
| Surface area, (m$^2$/g) | 94.53 |
| Particle porosity | 0.65 |
| Bed porosity | 0.45 |
| Average particle diameter, mm | 0.775 |
| Pore volume, (cm$^3$/g) | 0.544 |
| Chemical properties | |
| pH | 7.5 |
| Ash content, (%) | 12 |
| Cation exchange capacity, CEC (meq/100 g) | 51.15 |
| Organic volatile solid, (V.S, $10^6$ mg/l) | 0.135 |
| Non-volatile solid, (N.V.S, $10^6$ mg/l) | 0.018 |

size, $d_{50}$, of 180 μm and a uniformity coefficient, $C_u = d_{60}/d_{10}$, of 1.73.

Lead was selected as a representative of heavy metal contaminants. To simulate the water's lead contamination, a solution of $Pb(NO_3)_2$ (manufactured by BDH, England) was prepared and added to the specimen to obtain representative concentration.

### 2.2. Batch experiments

These tests were carried out to specify the best conditions of contact time, initial pH of the solution, initial concentration, dosage and agitation speed. Six flasks of 250 ml are employed. Each flask is filled with 100 ml of lead solution which has initial concentration of 50 mg/l. About 0.25 g of adsorbent was added into different flasks. These flasks were kept stirred in the high-speed orbital shaker at 250 rpm for different periods of time. A fixed volume (20 ml) of the solution was withdrawn from each flask. This withdrawn solution was filtered to separate the adsorbent and a fixed volume (10 ml) of the clear solution was pipetted out for the concentration determination of lead ions still present in solution. The measurements were carried out using atomic absorption spectrophotometer (AAS) (SHIMADZU, JAPAN). These measurements were repeated for two times and average value has been taken. However, the adsorbed concentration of metal ion on the reactive material was obtained by a mass balance. Kinetic studies were investigated with different values of pH (3, 4, 5, 6 and 7), initial concentration of $Pb^{2+}$ (50, 100, 150, 200 and 250 mg/l), adsorbent dosage (0.15, 0.25, 0.5, 1, 2 and 3 g per 100 ml) and agitation speed (0, 50, 100, 150, 200 and 250 rpm).

From the best experimental results, the amount of metal ion retained in the GDAS phase, $q_e$, was calculated using the following equation [19]:

$$q_e = (C_o - C_e)\frac{V}{m} \quad (1)$$

where $C_o$ and $C_e$ are the initial and equilibrium concentrations of lead in the solution (mg/l), $V$ is the volume of solution in the flask (L) and $m$ is the mass of GDAS in the flask (g).

### 2.3. Description of sorption data

Six isotherm models were used for the description of sorption data. A summary of these models was presented by Hamdaoui and Naffrechoux [20] as follows:

- *Langmuir model*: assumes uniform energies of adsorption onto the surface and no transmigration of adsorbate in the plane of the surface. It can be written as follows:

Table 2
Composition and properties of the soil used in the present study

| Property | Value |
|---|---|
| Particle size distribution (ASTM D 422) | |
| Sand (%) | 95 |
| Silt and clay (%) | 5 |
| Hydraulic conductivity(coefficient of permeability) (m s$^{-1}$) | $4.22 \times 10^{-5}$ |
| Cation exchange capacity (meq/100 g) | 1.56 |
| pH | 8.65 |
| Organic content (ASTM D 2974) (%) | 0.26 |
| Mass density (g/cm$^3$) | 2.65 |
| Bulk density (g/cm$^3$) | 1.563 |
| Porosity of aquifer ($n_A$) | 0.41 |
| Soil classification | Sand |

$$q_e = \frac{q_m b C_e}{1 + bC_e} \quad (2)$$

where $q_m$ is the maximum adsorption capacity (mg/g) and $b$ is the constant related to the free energy of adsorption (l/mg).

- *Freundlich model*: is quantified by:

$$q_e = K_F C_e^{1/n} \quad (3)$$

where $K_F$ is the Freundlich sorption coefficient and $n$ is an empirical coefficient indicative of the intensity of the adsorption.

- *Elovich model*: is based on a kinetic principle assuming that the adsorption sites increase exponentially with adsorption, which implies a multilayer adsorption. It can be expressed as follows:

$$\frac{q_e}{q_m} = K_E C_e \exp\left(-\frac{q_e}{q_m}\right) \quad (4)$$

where $K_E$ is the Elovich equilibrium constant (l/mg) and $q_m$ is the Elovich maximum adsorption capacity (mg/g).

- *Temkin model*: assumes that the heat of adsorption of all the molecules in the layer decreases linearly with coverage due to adsorbent–adsorbate interactions, and that the adsorption is characterized by a uniform distribution of the binding energies, up to some maximum binding energy. This model is given by:

$$\theta = \frac{RT}{\Delta Q} \ln K_o C_e \quad (5)$$

where $\theta$ ($=q_e/q_m$) is the fractional coverage, $R$ is the universal gas constant (kJ mol$^{-1}$ K$^{-1}$), $T$ is the

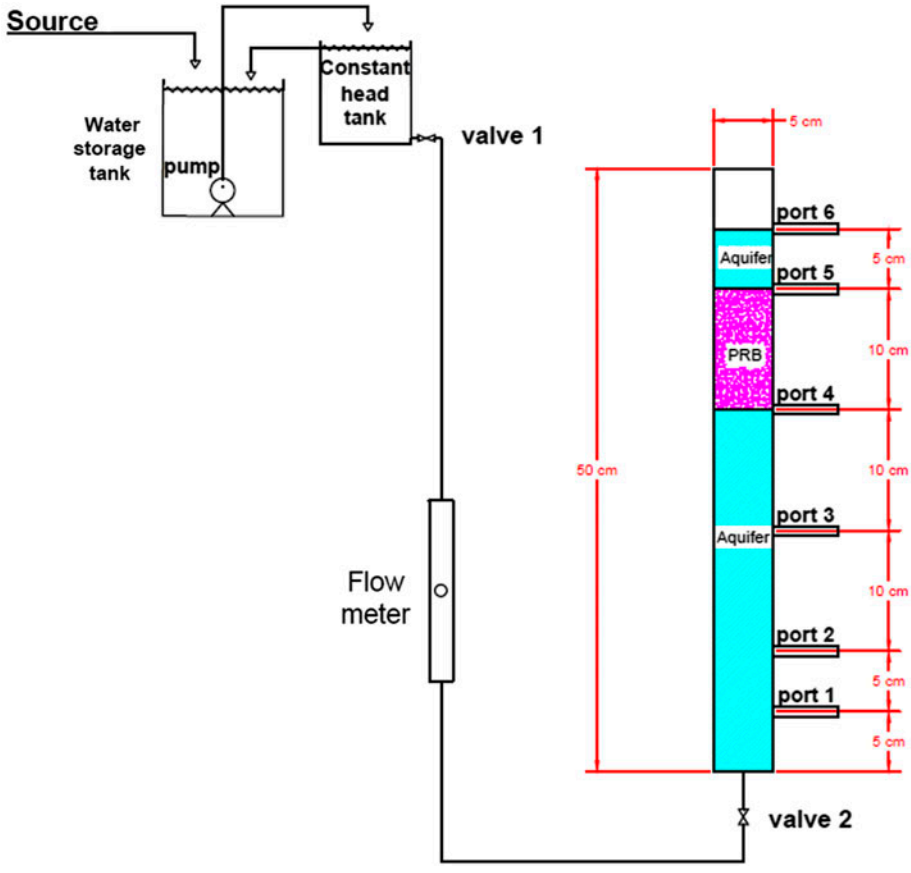


Fig. 1. Schematic diagram of the laboratory-scale column.

temperature (K), $\Delta Q$ is the variation of adsorption energy (kJ mol$^{-1}$) and $K_o$ is the Temkin equilibrium constant (l/mg).

- *Kiselev model*: is known as the adsorption isotherm in localized monomolecular layer and can be expressed by:

$$k_1 C_e = \frac{\theta}{(1-\theta)(1+k_n\theta)} \quad (6)$$

where $k_1$ is the Kiselev equilibrium constant (l/mg), $\theta$ ($=q_e/q_m$) is the fractional coverage and $k_n$ is the constant of complex formation between adsorbed molecules.

- *Hill–de Boer model*: describes the case where there are mobile adsorption and lateral interaction among adsorbed molecules. This model is given by:

$$k_1 C_e = \frac{\theta}{1-\theta} exp\left(\frac{\theta}{1-\theta} - \frac{k_2\theta}{RT}\right) \quad (7)$$

where $k_1$ is the Hill–de Boer constant (l/mg) and $k_2$ is the energetic constant of the interaction between adsorbed molecules (kJ/mol).

### 2.4. Continuous experiments

Fig. 1 shows the schematic diagram of the reactor set-up used in the present study. This set-up is constructed of Perspex cylinder having height and diameter equal to 50 and 5 cm, respectively. The column is equipped with six sampling ports at the distance of 5 (port 1), 10 (port 2), 20 (port 3), 30 (port 4), 40 (port 5) and 45 cm (port 6) from the bottom. These ports should be constructed of stainless steel fittings which blocked with Viton stoppers. Sampling was carried out at specified periods from sampling ports using needle to be inserted into the centreline of the column. The column was packed with sandy soil as aquifer and GDAS as barrier in the configuration and alignment illustrated in Fig. 1. Then, distilled water was fed slowly into the bottom of the column and forced upward through the medium, pushing the air in front of it. The contaminated solution with $Pb^{2+}$, which simulated the contaminated groundwater, was introduced into the column from certain reservoir. The flow rate from this reservoir, which is placed at the elevation higher than the level of column outlet, was controlled by valve 1, valve 2 and flow meter. Three values of flow rate (5, 10 and 15 ml/min) are selected and artificial contaminated water was flushed the column for each experiment. Monitoring of $Pb^{2+}$ concentration along the length of the column in the effluent from sampling ports was conducted for a period of 7 d. The water samples were taken regularly (after 1, 2, 5 and 7 d) and analysed by AAS. The filling material in the column was assumed to be homogeneous and incompressible and constant over time for water-filled porosity. All tubing and fitting for the influent and effluent lines should be composed of an inert material.

A tracer experiment, adopted the same procedure of Ujfaludi in 1986, was performed to determine the effective *Longitudinal* dispersion coefficient for the sandy soil and GDAS [21].

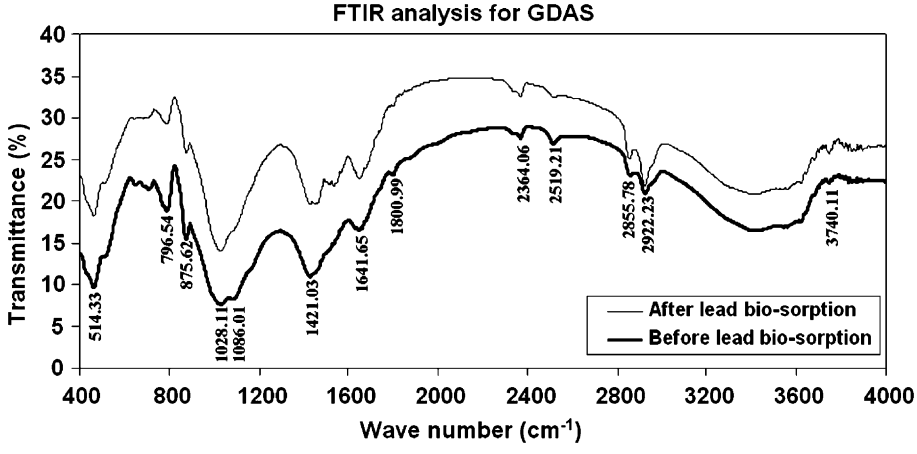


Fig. 2. FTIR spectra of GDAS before and after bio-sorption of lead.

## 3. Results and discussion

### 3.1. Fourier transform infrared (FTIR) analysis

This analysis has been considered as a kind of direct means for investigating the sorption mechanisms by identifying the functional groups responsible for metal binding [22]. Infrared spectra of GDAS samples before and after bio-sorption of $Pb^{+2}$ were examined using (SHIMADZU FTIR, 8000 series spectrophotometer). These spectra were measured within the range 400–4,000 $cm^{-1}$ as shown in Fig. 2. The infrared spectrum and functional group assigned for adsorption can be summarized as: 514.33 (alkyl halides), 796.54 (phosphines), 875.62 (aromatic), 1028.11 (alcohol, carboxylic acid), 1086.01 (alcohol), 1421.03 (carboxylic acid), 1641.65 (alkane), 1800.99 (carboxylic acid), 2364.06 (alkane), 2519.21 (carboxylic acid), 2855.78 (alkane), 2922.23 (alkane) and 3740.11 (carboxylic acid) [23].

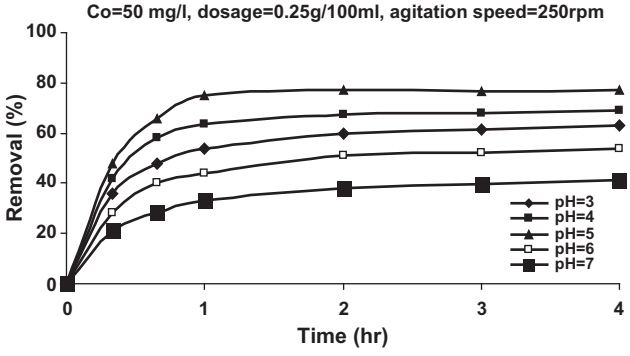


Fig. 3. Removal efficiency of lead on GDAS as a function of contact time and initial pH.

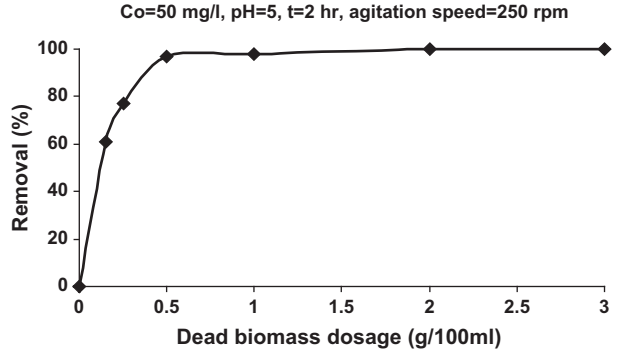


Fig. 4. Effect of GDAS dosage on removal efficiencies of $Pb^{+2}$.

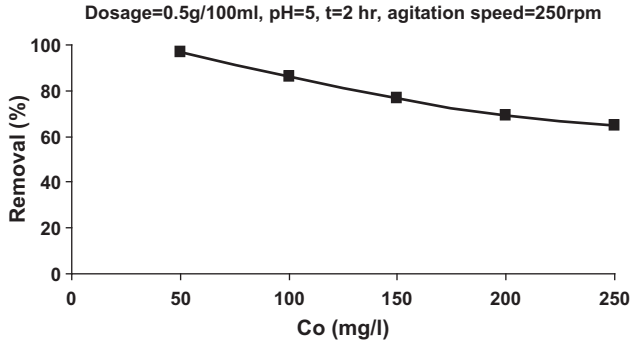


Fig. 5. Effect of initial concentration on removal efficiency of $Pb^{+2}$ on GDAS.

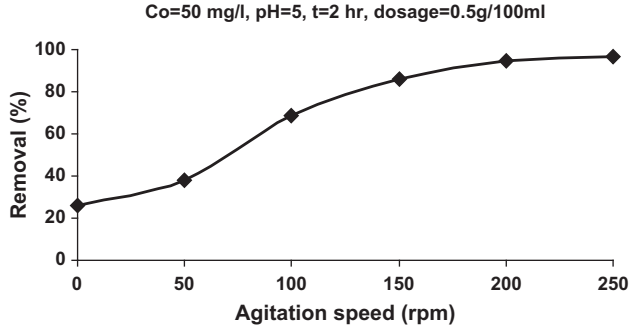


Fig. 6. Effect of agitation speed on percentage removal of $Pb^{+2}$.

Table 3
Parameters of isotherm models for the bio-sorption of $Pb^{2+}$ onto GDAS and soil

| | | $Pb^{+2}$ ions | |
|---|---|---|---|
| Isotherm model | Parameter | GDAS | Soil |
| Langmuir | $b$ (l/mg) | 0.0349 | 0.0133 |
| | $q_m$ (mg/mg) | 0.1116 | 0.0308 |
| | $R^2$ | 0.9914 | 0.9893 |
| Freundlich | $K_F$ (mg/mg)(l/mg)$^{1/n}$ | 0.0079 | 0.0016 |
| | $n$ | 3.0650 | 2.5893 |
| | $R^2$ | 0.9893 | 0.8623 |
| Elovich | $q_m$ (mg/mg) | 0.0090 | – |
| | $K_E$ (l/mg) | 1.4670 | |
| | $R^2$ | 0.9555 | |
| Temkin | $\Delta Q$ (kJ/mole) | 14.6770 | – |
| | $K_o$ (l/mg) | 1.0009 | |
| | $R^2$ | 0.9658 | |
| Kiselev | $k_1$ (l/mg) | 0.2785 | – |
| | $k_n$ | −0.8790 | |
| | $R^2$ | 0.9123 | |
| Hill-de Boer | $k_1$ (l/mg) | 0.0136 | – |
| | $k_2$ (kJ/mole) | 24.7274 | |
| | $R^2$ | 0.9345 | |

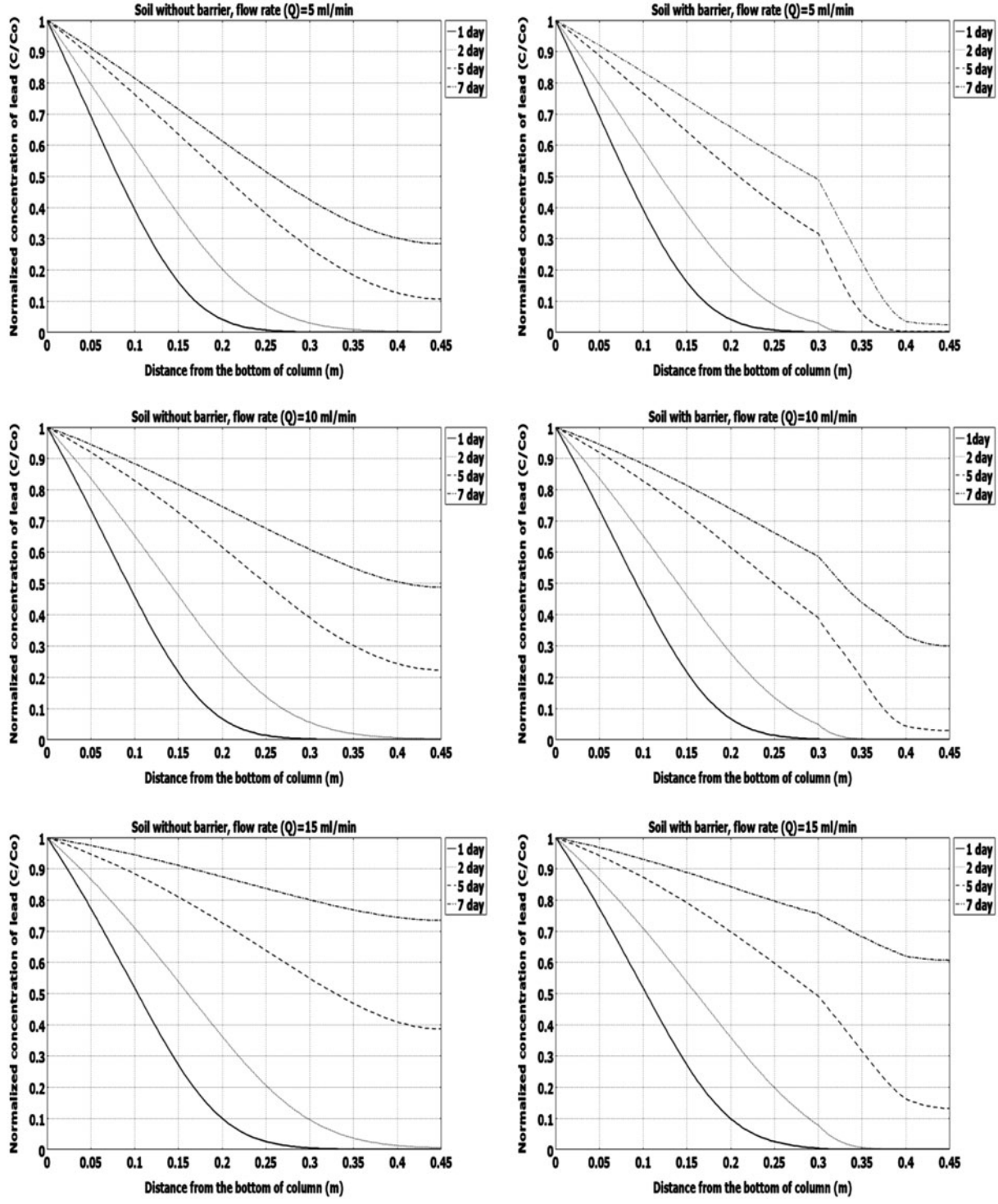


Fig. 7. Calculated normalized concentration of lead along the length of the column with and without presence of PRB at different values of flow rate.

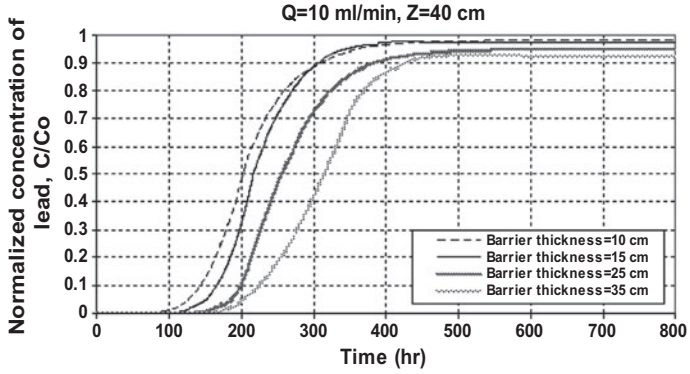


Fig. 8. Normalized concentration vs. time of various PRB thickness.

### 3.2. Influence of batch operating parameters

#### 3.2.1. Effect of contact time and initial pH of solution

Fig. 3 shows the effect of contact time and initial pH of solution on lead sorption using 0.25 g of GDAS added to 100 ml of metal solution for batch tests at 25°C. This figure shows that the adsorption rate was very fast initially and it increased with increasing of contact time until reached the equilibrium time (= 2 h). This may be due to the presence of large number of adsorbent sites available for the adsorption of metal ions. As the remaining vacant surfaces decreasing, the adsorption rate slowed down due to formation of replusive forces between the metals on the solid surfaces and in the liquid phase [24]. Also, the increase in the metal removal as the pH increases can be explained on the basis of a decrease in competition between proton and metal species for the surface sites, and the decrease in positive surface charge, which results in a lower columbic repulsion of the sorbing metal [25]. However, further increase in pH values would cause a decreasing in removal efficiency. This may be attributed to the formation of soluble hydroxy complexes which are precipitated from the solution making true sorption studies impossible [26]. It is clear from this figure that the maximum removal efficiency of lead was achieved at initial pH of 5.

#### 3.2.2. Effect of GDAS weight

Fig. 4 presents the removal efficiency of $Pb^{+2}$ as a function of different weights of GDAS ranged from 0.15 to 3 g added to 100 ml of metal solution. It can be observed that removal efficiency of the GDAS improved with increasing adsorbent dosage from 0.15 to 0.5 g for a fixed initial metal concentration. This was expected due to the fact that the higher dose of adsorbents in the solution, the greater availability of sorption sites.

#### 3.2.3. Effect of initial lead concentration

Fig. 5 explains that the removal efficiency of $Pb^{+2}$ decreased from 97 to 65% with increasing the initial concentration from 50 to 250 mg/l. This figure represents saturation of the active sites available on the GDAS samples for interaction with ions of contaminant. These results indicate that energetically less favourable sites become involved with increasing concentrations in the aqueous solution [27].

#### 3.2.4. Effect of agitation speed

Fig. 6 shows that about 26% of the lead was removed before shaking (agitation speed= zero) and the uptake increases with the increase of shaking rate. There was gradual increase in contaminants uptake when agitation speed was increased from 0 to 250 rpm at which about 97% of $Pb^{+2}$ has been removed. This can be attributed to improving the diffusion of ions towards the surface of the reactive media and, consequently, proper contact between ions in solution and the binding sites can be achieved.

### 3.3. Sorption isotherms

The sorption data for lead ions on GDAS are fitted with a linearized form of (Langmuir, Freundlich, Temkin, Elovich, Kiselev and Hill-de Boer) models adopted here. Additionally, the sorption data of sandy soil are fitted only with Langmuir and Freundlich models. Table 3 presents the fitted parameters and coefficient of determination ($R^2$) for each model. It is clear that the Langmuir isotherm model provided the best correlation in compared with other models for lead bio-sorption on the GDAS and soil. Accordingly, the Langmuir isotherm model will be used to describe the sorption of lead on these media in the partial differential equation (PDE) governed the transport of a solute in the continuous mode.

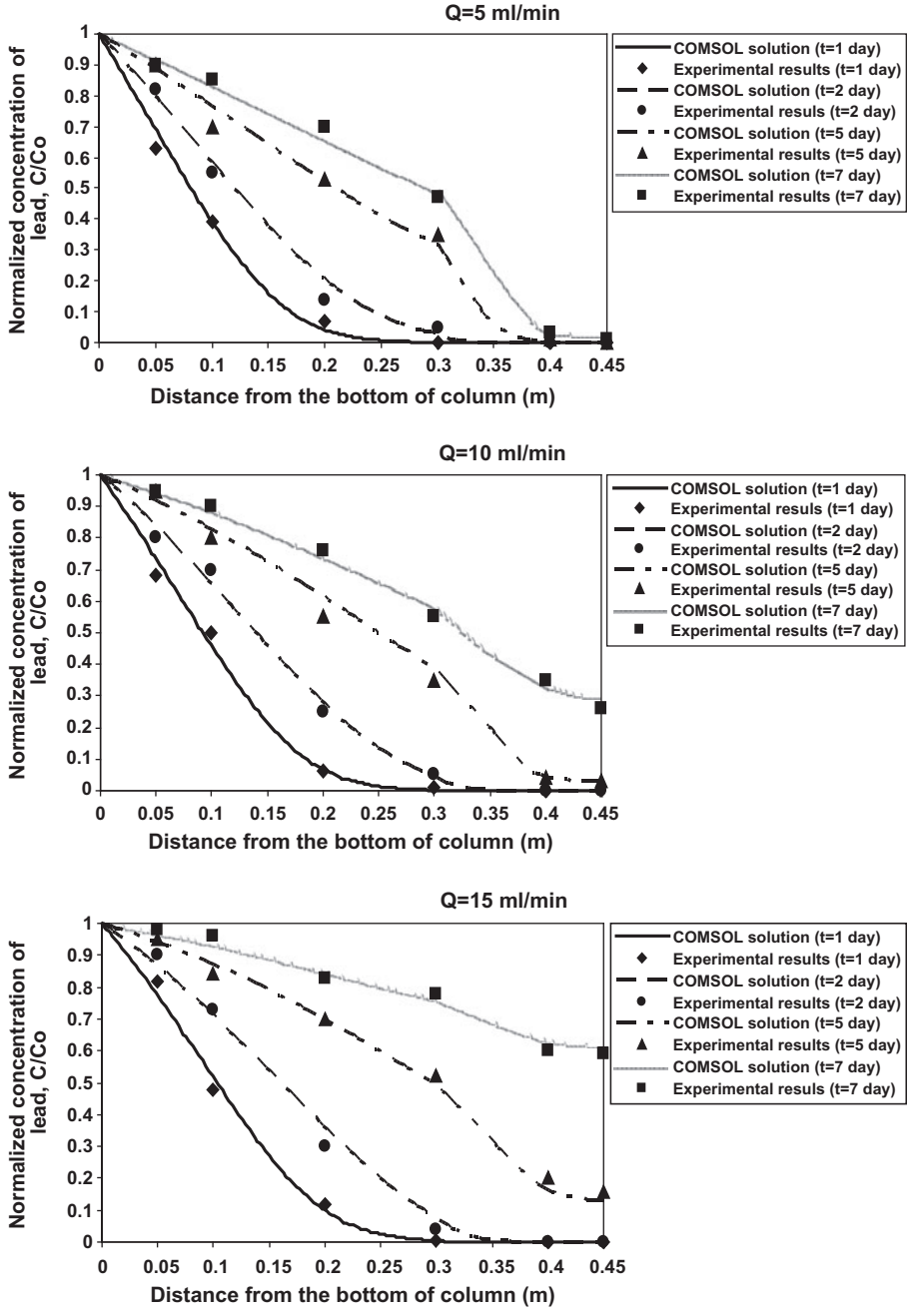


Fig. 9. Comparison between COMSOL predictions and experimental results for $Pb^{+2}$ concentrations in groundwater.

### 3.4. Longitudinal dispersion coefficient

Results of the experimental runs concerned the measurement of longitudinal dispersion coefficient ($D_L$) at different values of velocity ($V$) for soil and GDAS are taken a linear relationship as follows:

$$D_L = 6.490\,V + 0.5325 \quad R^2 = 0.9960 \quad \text{for soil} \tag{8}$$

$$D_L = 17.511\,V + 0.0225 \quad R^2 = 0.9903 \quad \text{for GDAS} \tag{9}$$

These equations are taken the general form of longitudinal hydrodynamic dispersion coefficient as follows:

$$D_L = \alpha_L V + D^* \tag{10}$$

*where $D^*$ is the effective molecular diffusion coefficient*. This means that the longitudinal dispersivity ($\alpha_L$) is equal to 6.49 cm for soil and 17.511 cm for GDAS.

### 3.5. Modelling application

The contaminant migration in a porous medium is due to advection–dispersion processes; therefore, considering a 1D system, the dissolved lead mass balance equation may be written, as follows [28]:

$$D_z \frac{\partial^2 C_{Pb}}{\partial z^2} - V_z \frac{\partial C_{Pb}}{\partial z} = \frac{\partial C_{Pb}}{\partial t} + \frac{\rho_b}{n}\frac{\partial q}{\partial t} \quad (11)$$

where $D_z$ *is the dispersion coefficient in the direction z*, $V_z$ *is the velocity of flow*, $C_{Pb}$ represents lead mass concentration in water, $q$ the lead concentration on solid and $\rho_b$ the dry adsorbing material bulk density.

Under isotherm conditions, $q$ in the second term on the right hand side of this equation can be substituted by Langmuir model (Eq. 2). The initial liquid and solid lead concentrations are assumed to be zero throughout the entire flow domain and the boundary conditions used in COMSOL Multiphysics 3.5a are reported in Eq. (12):

$$\text{Lower boundary}(@\ z = 0) : C_{Pb} = 50\,\text{mg/l}$$

$$\text{Upper boundary}(@\ z = 45\text{cm}) : \text{advective flux } \left(\text{i.e.}\frac{\partial C_{Pb}}{\partial z} = 0\right) \quad (12)$$

Interior boundaries in the barrier zone (i.e. @ $z = 30$ and 40 cm): continuity.

Fig. 7 reports the concentration lines of lead in the aquifer, calculated by COMSOL package, with and without presence of PRB at flow rate equal to 5, 10 and 15 ml/min after many time intervals. This figure illustrates the important role of the barrier in restricting the propagation of contaminant plume. It also seems that the increased value of flow rate will increase the velocity of flow and, consequently, this will increase the propagation of contaminant front.

Effect of PRB thickness, varied from 10 to 35 cm, on lead treatment in the down gradient of barrier ($z = 40$ cm) for flow rate equal to 10 ml/min as the example illustrated in Fig. 8. It is clear that thicker PRB shows better lead treatment than the thinner ones. The thicker PRB provides better lead treatment performance because the lead solution has greater retention time that allows better adsorption process in the PRB. However, it seems that this barrier starts to saturate with increasing the travel time and this means that the lead retardation factor was reduced, indicating a decrease in the percentage of GADS functionality for contaminant retardation.

Comparison between the predicted and experimental results for $Pb^{+2}$ concentrations during the migration of the contaminant plume at different values of time periods and flow rates along the tested column are depicted in Fig. 9. It is clear from this figure that there is a good agreement between these results with root mean square error (RMSE) [29] not exceeded the 0.0499.

## 4. Conclusions

(1) Contact time, initial pH of the solution, initial metal ion concentration, GDAS dosage and agitation speed were most of the parameters affected on the sorption process between $Pb^{+2}$ ions and GDAS. The best values of these parameters that will achieve the maximum removal efficiency of $Pb^{+2}$ (=97%) were 2 h, 5, 50 mg/l, 0.5 g/100 ml and 250 rpm, respectively.

(2) Lead sorption data on the GDAS and soil were correlated reasonably well by the Langmuir sorption isotherm with coefficient of determination ($R^2$) equal to 0.9914 and 0.9893, respectively.

(3) FTIR analysis proved that the alkyl halides, phosphines, aromatic, alcohol, carboxylic acid and alkane groups are responsible for the biosorption of lead onto GADS.

(4) The results of 1D numerical model, solved by COMSOL Multiphysics 3.5a under equilibrium condition, proved that the GDAS barrier is efficient technique in the restriction of contaminant plume. These results explained that the thicker PRB shows better lead treatment than the thinner ones and the barrier starts to saturate with contaminant as a function of the travel time. A good agreement between the predicted and experimental results was recognized with RMSE not exceeded the 0.0499.

## References

[1] US Environmental Protection Agency (USEPA), How to Evaluate Alternative Cleanup Technologies for Underground Storage Tank Sites, EPA 510-95-007, Washington, DC, 1995.

[2] C.C. Travis, C.B. Doty, ES&T views: Can contaminated aquifers at superfund sites be remediated? Environ. Sci. Technol. 24 (1990) 1464–1466.
[3] R.W. Gillham, D.R. Burris, Recent developments in permeable *in situ* treatment walls for remediation of contaminated groundwater, Proceedings of the Subsurface Restoration Conference, Dallas, TX, June 21–24, 1992.
[4] National Research Council, Alternatives for Ground Water Cleanup, National Academies Press, Washington, DC, 1994, p. 315.
[5] R.W. Puls, R.M. Powell, D.W. Blowes, J.L. Vogan, R.W. Gillham, P.D. Powell, D. Schultz, T.M. Sivavec, R. Landis, Permeable Reactive Barriers Technologies for Contaminant Remediation, United States Environmental Protection Agency, Report, # EPA/600/R-98/125, Washington, DC, 1998.
[6] J.B. Park, S.H. Lee, J.W. Lee, C.Y. Lee, Lab scale experiments for permeable reactive barriers against contaminated groundwater with ammonium and heavy metals using clinoptilolite (01-29B), J. Hazard. Mater. 95 (2002) 65–79.
[7] A.Z. Woinarski, I. Snape, G.W. Stevens, S.C. Stark, The effects of cold temperature on copper ion exchange by natural zeolite for use in a permeable reactive barrier in Antarctica, Cold Reg. Sci. Technol. 37 (2003) 159–168.
[8] B. Yuncu, F.D. Sanin, U. Yetis, An investigation of heavy metal biosorption in relation to C/N ratio of activated sludge, J. Hazard. Mater. 137 (2006) 990–997.
[9] F. Di Natale, M. Di Natale, R. Greco, A. Lancia, C. Laudante, D. Musmarra, Groundwater protection from cadmium contamination by permeable reactive barriers, J. Hazard. Mater. 160 (2008) 428–434.
[10] M.R. Boni, S. Sbaffoni, The potential of compost-based biobarriers for Cr(VI) removal from contaminated groundwater: Column test, J. Hazard. Mater. 166 (2009) 1087–1095.
[11] A. Hanif, H.N. Bhatti, M.A. Hanif, Removal and recovery of Cu(II) and Zn(II) using immobilized Mentha arvensis distillation waste biomass, Ecol. Eng. 35 (2009) 1427–1434.
[12] G. Bartzas, K. Komnitsas, Solid phase studies and geochemical modelling of low-cost permeable reactive barriers, J. Hazard. Mater. 183 (2010) 301–308.
[13] P.S. Calabrò, N. Moraci, P. Suraci, Estimate of the optimum weight ratio in zero-valent iron/pumice granular mixtures used in permeable reactive barriers for the remediation of nickel contaminated groundwater, J. Hazard. Mater. 207–208 (2012) 111–116.
[14] A.A. Faisal, Z.A. Hmood, Groundwater protection from cadmium contamination by zeolite permeable reactive barrier, Desalin. Water Treat. doi: 10.1080/19443994.2013.855668.
[15] C.S. Zhu, L.P. Wang, W. Chen, Removal of Cu(II) from aqueous solution by agricultural by-product: Peanut hull, J. Hazard. Mater. 168 (2009) 739–746.
[16] M.W. Wan, C.C. Kan, B.D. Rogel, M.L.P. Dalida, Adsorption of copper(II) and lead(II) ions from aqueous solution on chitosan-coated sand, Carbohydr. Polym. 80 (2010) 891–899.
[17] W.D. Robertson, Nitrate removal rates in woodchip media of varying age, Ecol. Eng. 36 (2010) 1581–1587.
[18] A. Mathews, I. Zayas, Particle size and shape effects on adsorption rate parameters, J. Environ. Eng. 115 (1989) 41–55.
[19] S. Wang, Z. Nan, Y. Li, Z. Zhao, The chemical bonding of copper ions on kaolin from Suzhou, China, Desalination 249 (2009) 991–995.
[20] O. Hamdaoui, E. Naffrechoux, Modeling of adsorption isotherms of phenol and chlorophenols onto granular activated carbon, J. Hazard. Mater. 147 (2007) 381–394.
[21] L. Ujfaludi, Longitudinal dispersion tests in non-uniform porous media, Hydrol. Sci. J. 31 (1986) 467–474.
[22] J.P. Chen, L. Wang, S.W. Zou, Determination of lead bio-sorption properties by experimental and modeling simulation study, Chem. Eng. J. 131 (2008) 209–215.
[23] K.M. Doke, M. Yusufi, R.D. Joseph, E.M. Khan, Biosorption of hexavalent chromium onto wood apple shell: Equilibrium, kinetic and thermodynamic studies, Desalin. Water Treat. 50 (2012) 170–179.
[24] G.O. El-Sayed, H.A. Dessouki, S.S. Ibrahim, Biosorption of Ni(II) and Cd(II) ions from aqueous solutions onto rice straw, Chem. Sci. J. 9 (2010) 1–11.
[25] M. Alkan, B. Kalay, M. Doğan, Ő. Demirbaş, Removal of copper ions from aqueous solutions by kaolinite and batch design, J. Hazard. Mater. 153 (2008) 867–876.
[26] C. Raji, G.N. Manju, T.S. Anirudhan, Removal of heavy metal ions from water using sawdust-based activated carbon, Indian J. Eng. Mater. 4 (1997) 254–260.
[27] M. Selvarani, P. Prema, Removal of toxic metal hexavalent chromium [Cr(VI)] from aqueous solution using starch—Stabilized nanoscale zero valent iron as adsorbent: equilibrium and kinetics, Int. J. Environ. Sci. 2 (2010) 1962–1975.
[28] L.N. Reddi, H.I. Inyang, Geoenvironmental Engineering Principles and Applications, Marcel Dekker, New York, NY, 2000, ISBN: 0-8247-0045-7.
[29] M.P. Anderson, W.W. Woessner, Applied Groundwater Modeling: Simulation of Flow and Advective Transport, second ed., Academic Press, San Diego, CA, 1992.